Heliyon 9 (2023) e21174

Contents lists available at ScienceDirect

Heliyon

journal homepage: www.cell.com/heliyon

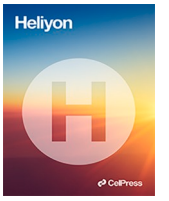

Inflammation-related signature for prognostic prediction, tumor immune, genomic heterogeneity, and drug choices in prostate cancer: Integrated analysis of bulk and single-cell RNA-sequencing

Weian Zhu [a,1], Jiongduan Huang [a,1], Jianjie Wu [a], Chenglun Wu [a], Fengxi Ye [b], Xiang Li [c,*], Wenjie Lai [d,a,**]

[a] Department of Urology, The Third Affiliated Hospital, Sun Yat-sen University, Guangzhou, 510630, China
[b] Zhongshan School of Medicine, Sun Yat-sen University, Guangzhou, 510080, China
[c] Department of Emergency Medicine, Nanfang Hospital, Southern Medical University, Guangzhou, 510515, China
[d] Laboratory of Biomaterials and Translational Medicine, Center for Nanomedicine, The Third Affiliated Hospital, Sun Yat-sen University, Guangzhou, 510630, China

ARTICLE INFO

Keywords:
Prostate cancer
Inflammation
Prognostic signature
Single-cell RNA-Sequencing
Tumor immune
Genomic heterogeneity
Drug choices

ABSTRACT

Background: Prostate cancer (PCa) ranks as the second most prevalent malignancy among males on a global scale. Accumulating evidence suggests that inflammation has an intricate relationship with tumorigenesis, tumor progression and tumor immune microenvironment. However, the overall impact of inflammation-related genes on the clinical prognosis and tumor immunity in PCa remains unclear.

Methods: Machine learning methods were utilized to construct and validate a signature using The Cancer Genome Atlas (TCGA) for training, while the Memorial Sloan Kettering Cancer Center (MSKCC) and GSE70769 cohorts for independent validation. The efficacy of the signature in predicting outcomes and its clinical utility were assessed through a series of investigations encompassing in vitro experiments, survival analysis, and nomogram development. The association between the signature and precision medicine was explored via tumor immunity, genomic heterogeneity, therapeutic response, and molecular docking analyses, using bulk and single-cell RNA-sequencing data.

Results: We identified 7 inflammation-related genes with prognostic significance and developed an inflammation-related prognostic signature (IRPS) with 6 genes. Furthermore, we demonstrated that both the IRPS and a nomogram integrating risk score and pathologic T stage exhibited excellent predictive ability for the survival outcomes in PCa patients. Moreover, the IRPS was found to be significantly associated with the tumor immune, genomic heterogeneity, therapeutic response, and drug selection.

Conclusion: IRPS can serve as a reliable predictor for PCa patients. The signature may provide clinicians with valuable information on the efficacy of therapy and help personalize treatment for PCa patients.

* Corresponding author. Department of Emergency Medicine, Nanfang Hospital, Southern Medical University, Guangzhou, 510515, China.
** Corresponding author. Department of Urology, The Third Affiliated Hospital, Sun Yat-sen University, Guangzhou, 510630, China.
E-mail addresses: li920402@smu.edu.cn (X. Li), laiwj28@mail.sysu.edu.cn (W. Lai).
[1] These authors contributed equally to this work: Weian Zhu, Jiongduan Huang.

https://doi.org/10.1016/j.heliyon.2023.e21174
Received 24 April 2023; Received in revised form 10 September 2023; Accepted 17 October 2023
Available online 18 October 2023

1. Introduction

Prostate cancer (PCa), with a rising incidence in recent years, stands as the second most prevalent malignant tumor in males worldwide [1,2]. Despite improvements in comprehensive treatment strategies, 25 % of treated men experience biochemical recurrence (BCR) [3,4]. While clinical assessments like prostate-specific antigen (PSA), Gleason score, and clinical stage provide some insight into a patient's prognosis, they are often limited, and patients with similar clinical conditions may have different prognoses [5]. Consequently, there is a pressing need to investigate novel prognostic indicators and develop more accurate prognostic models to predict the clinical outcomes and guide individualized treatment in PCa patients.

Chronic inflammation, which produces cytokines that promote tumor proliferation and metastasis, disrupt adaptive immunity, and reduce the effectiveness of cancer treatment, has been linked to cancer occurrence and development [6,7]. In recent years, the function of cancer-related inflammation in carcinogenesis and tumor growth have become hot topics of research, and has been categorized as the eighth characteristic of cancer [8]. Inflammation has been identified as a key driver of the occurrence and progression of PCa [9]. Previous studies suggest that inflammatory damage may contribute to the tumorigenesis of PCa by inducing cellular stress and causing repeated genomic damage [10,11]. However, there is currently no reliable model in PCa patients for predicting biochemical recurrence-free survival (bRFS) specifically using inflammation-related genes (IRGs).

The tumor microenvironment (TME), recognized as a complex multicellular setting for carcinogenesis, has been generally acknowledged to affect tumor growth and treatment outcomes [12]. Inflammation has been shown to influence the cellular composition of various components within the TME [13]. It can promote the development of PCa by driving androgen receptor signals and repairing DNA defects, with immune and senescent cells in the TME amplifying this process. Additionally, inflammation can contribute to tumor immune escape in PCa by selecting certain cells and components within the TME [14]. Moreover, immune cells in the innate and acquired immune systems, such as dendritic cells, natural killer cells, macrophages, and B cells, have been implicated in tumor growth and immunotherapeutic response [15]. A comprehensive understanding of immune infiltration components in the TME holds paramount importance in increasing the response rate and developing new cancer immunotherapies [16,17]. Fortunately, single-cell RNA-sequencing (scRNA-seq), a cutting-edge technique, not only enables simultaneous assessment of thousands of cells in a sample but also unveils intricate heterogeneity among tumor cells and the TME complexity [18]. In recent years, this methodology has gained widespread application in investigating the tumor characteristics and clinical treatment in PCa [19,20]. Hence, further exploration of PCa therapy biomarkers is imperative.

In our study, our objective was to construct and verify an inflammation-related prognostic signature (IRPS) for predicting bRFS in patients with PCa through experiments, as well as bulk and scRNA-seq analysis. In addition, we conducted a comprehensive evaluation of the predictive and prognostic value, the link with the TME and genomic heterogeneity, and the importance of antineoplastic drug selection of the novel PCa model. The findings of this study may improve prediction accuracy and therapeutic effect in PCa patients.

2. Materials and methods

2.1. Public data sources and preprocessing

Publicly available RNA-seq, copy number variation (CNV), mutation, and corresponding clinical data were collected from The Cancer Genome Atlas (TCGA) database (https://portal.gdc.cancer.gov/) [21] as a training cohort. Additionally, gene expression and clinical information of two independent validation cohorts were collected from the Memorial Sloan Kettering Cancer Center (MSKCC, https://www.mskcc.org/) [22] and GSE70769 (https://www.ncbi.nlm.nih.gov/bioproject/PRJNA289512) [23], respectively. All datasets were independent, and the batch effect was eliminated using the "LIMMA" and "SVA" packages. Meanwhile, the gene sets of IRGs, including 200 genes (Table S1), were extracted from the Molecular Signatures Database (https://www.gsea-msigdb.org/gsea/msigdb/) [24].

2.2. Screening for differentially expressed and prognostic IRGs

Differentially expressed genes (DEGs) related to inflammation between PCa samples and normal samples were identified in the TCGA cohort using the Wilcoxon rank-sum test in the R package of "LIMMA" (false discovery rate <0.05). Prognostic IRGs were further identified by the univariate Cox method.

2.3. Construction and verification of the IRPS

Firstly, the "VENN" package was used to obtain the intersection of DEGs related to inflammation and prognostic IRGs. Next, an interaction network was then constructed using data from the STRING database (https://string-db.org/) [25], and subsequently visualized in Cytoscape (version 3.8.2) [26]. Subsequently, a prognostic risk signature was developed by least absolute shrinkage and selection operator (LASSO)-Cox regression analysis using the R packages "GLMNET" and "SURVIVAL". The risk score for each patient was computed by summing the product of expression level and corresponding coefficient for each gene within the model. Patients were categorized into two groups, distinguished by low or high risk scores, based on the median threshold. Furthermore, principal component analysis (PCA) and t-distributed stochastic neighbor embedding (t-SNE) were employed with the assistance of the "STATS" and "RTSNE" to detect internal relationships between risk groups. Receiver operator characteristic (ROC) and Kaplan-Meier survival

curves were generated through "TIMEROC", "SURVMINER" and "SURVIVAL". Signature accuracy and generalization were verified in the MSKCC and GSE70769 cohorts through the same methods.

In order to further assess the validity of the IRPS in both the TCGA and MSKCC cohorts, a relationship analysis was conducted between clinicopathological features and risk score, as well as a survival study stratified by subgroup.

2.4. Real-time quantitative PCR (RT-qPCR)

A total of 40 fresh tissue samples, comprising 20 samples each of benign prostatic hyperplasia (BPH) and PCa specimens, were collected at the Third Affiliated Hospital of Sun Yat-sen University in Guangzhou, China, between 2021 and 2022. Sample acquisition followed informed consent procedures and received approval from the clinical ethics board. Using standard protocols [27], total RNA was extracted with TRIzol (Invitrogen) and subjected to reverse transcription using SuperScript™ III Reverse Transcriptase (Invitrogen). Subsequently, quantitative experiment was performed with SYBR Green qPCR reagent (GenStar) using GAPDH as an internal control. RT-qPCR primer sequences are listed in Table S2.

2.5. Immunohistochemistry (IHC) analysis

To validate differential protein expression of the model genes in PCa versus normal prostate samples, IHC data and images were obtained and assessed from the Human Protein Atlas (https://www.proteinatlas.org/) [28], a protein expression database.

2.6. Construction and assessment of nomogram

Harrell's C-index was used to investigate the connection between clinical variables and risk score within both TCGA and MSKCC cohorts. Furthermore, a nomogram was constructed to predict 1 year, 3 years, and 5 years bRFS utilizing "RMS" package and Cox regression coefficients. Nomogram accuracy and discrimination were evaluated through calibration, ROC and decision curve analysis (DCA) curves.

2.7. Functional analysis

The DEGs between the low- and high-risk groups were determined by Gene Ontology (GO) and Kyoto Encyclopedia of Genes and Genomes (KEGG) analyses, facilitated by the package of "CLUSTERPROFILER" in R [29]. *P*-values were adjusted using the Benjamini-Hochberg method.

2.8. scRNA-seq analysis

The scRNA-seq data of nine PCa samples were retrieved from GSE143791 (https://www.ncbi.nlm.nih.gov/geo/query/acc.cgi?acc=GSE143791), and objects were constructed and poor-quality cells were eliminated during the typical data preprocessing steps using the "SEURAT" program. Filtering criteria were applied, which included removing genes detected in <3 cells, cells with <50 detected genes, or cells with >5 % mitochondrial genes. Data were normalized by "LOGNORMALIZE", and the top 1500 highly variable genes were identified and subjected to PCA. The top 15 PCA were clustered and visualized in t-SNE using the "FINDCLUSTERS" and "TSNE" functions. Finally, the grouping and distribution of cells were annotated and analyzed using the "SINGLER" method.

2.9. Immune landscape analysis

The immune infiltration scores between risk groups, based on the model genes, were computed using various algorithms including EPIC [30], XCell [31], MCPCOUNTER [32], QUANTISEQ [33], CIBERSORT-ABS, CIBERSORT [34], and TIMER [35]. In addition, infiltration scores of 29 immune pathways and cells were then computed by the ssGSEA algorithm, facilitated by the R package "GSVA", and assessed with the Mann-Whitney test. Immune gene sets are listed in Table S3. Furthermore, we estimated and compared ESTIMATE score, immune score, stromal score, and tumor purity between risk groups, utilizing the package of "ESTIMATE" in R [36]. Finally, the score reflecting the 7 steps in the cancer-immunity cycle, derived from the IRPS, were assessed using Tracking Tumor Immunophenotype tool (https://biocc.hrbmu.edu.cn/TIP/), in accordance with a prior study [37].

2.10. Genomic heterogeneity analysis

Somatic mutation data and tumor mutation burden (TMB) data between risk groups were analyzed using the R package "MAFTOOLS". CNV data was calculated using GenePattern (https://www.genepattern.org/modules/docs/GISTIC_2.0) [38]. Associations between the IRPS-based risk score and markers of genomic heterogeneities, encompassing RNA-modified genes (Table S4), neoantigens, ploidy, loss of heterozygosity (LOH), mutant-allele tumor heterogeneity (MATH), microsatellite instability (MSI), and homologous recombination defect (HRD) from prior studies [39], were compared and examined.

2.11. Therapeutic efficacy analysis

The relationship between risk score and 46 immune checkpoints, as collected from a prior study [39], was compared. Immunophenoscore of PCa samples from TCGA was obtained through The Cancer Immunome Atlas (https://tcia.at/) [40] to compare PD1 and CTLA4 responses between risk groups. Anti-cancer drug sensitivity between risk groups was estimated using "PRROPHETIC" in R and IC50 values from the Genomics of Drug Sensitivity in Cancer (https://www.cancerrxgene.org/) [41]. In addition, pharmacological information regarding anti-cancer drug targets was obtained from DrugBank (https://go.drugbank.com/) database [42] and analyzed. The target genes of anti-tumor drugs are listed in Table S5.

To evaluate binding energy and interactions, IRPS gene coordinates were retrieved from the Protein Data Bank (http://www.rcsb.org/pdb/home/home.do) [43] and drug structures were obtained from PubChem Compound (https://pubchem.ncbi.nlm.nih.gov/) [44]. Water molecules were removed and polar hydrogens added to protein and ligand files in Molecular Operating Environment (version 2019.0102). Finally, molecular docking and visualization were performed.

2.12. Statistical analysis

Statistical analyses and graphical visualizations in the study were conducted using R software (version 4.2.1). Quantitative variables with a normal distribution were subjected to analysis via the independent *t*-test, whereas non-normally distributed quantitative variables were assessed using the Wilcoxon test. Ordinal categorical variables were analyzed through one-way ANOVA, and non-ordinal categorical variables were evaluated using the Kruskal-Wallis test. Statistically significant results were denoted by P values < 0.05, with levels of significance indicated as follows: $^{*}P < 0.05$, $^{**}P < 0.01$, $^{***}P < 0.001$, $^{****}P < 0.0001$, while "ns" signified non-significance.

3. Results

The flowchart of our study is depicted in Fig. 1. Simultaneously, the main clinicopathological characteristics of PCa patients enrolled in this study are listed in Table 1.

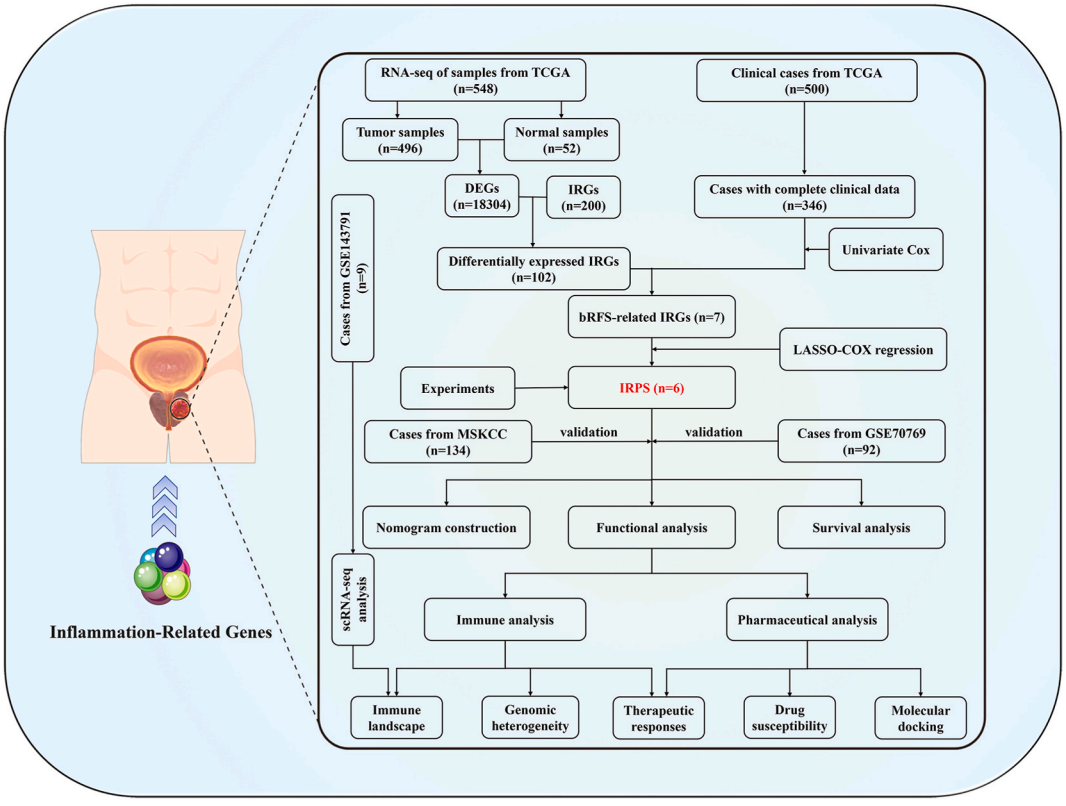

Fig. 1. The flow chart of the present study.

Table 1
Clinicopathological characteristics of the PCa patients included in this study.

Variables	TCGA cohort	MSKCC cohort	GSE70769 cohort
Age (years)			
≤65	247	113	
>65	99	21	–
Gleason Score			–
≤7	190	123	
>7	156	11	–
Status			–
BCR	37	31	45
Non-BCR	309	103	47
Pathologic T stage			
T1/T2	121	85	–
T3/T4	225	49	–

BCR, biochemical recurrence.

3.1. Identification of prognostic IRGs in the TCGA cohort

A total of 18304 DEGs were obtained by comparing 496 tumor samples with 52 normal samples sourced from the TCGA database. Then, by intersecting these DEGs with IRGs, we obtained 102 DEGs associated with inflammation. Among these, 7 genes, namely CD55, CDKN1A, INHBA, KCNJ2, PIK3R5, PTGIR, and TNFSF10, were related to bRFS through a univariate Cox regression analysis (Fig. 2A–C). The interrelationships among these bRFS-related DEGs were visualized using Cytoscape (Fig. 2D).

3.2. Construction and verification of the IRPS

To further identify the genes with prognostic values from the 7 candidates, we employed the LASSO-Cox regression method to derive an optimal prognosis model. Then, 6 genes, namely CD55, CDKN1A, INHBA, KCNJ2, PTGIR, and TNFSF10, were screened out based on the penalty parameter (λ) determined via the minimum criteria (Fig. 3A). Through detection of mRNA expression levels of 6

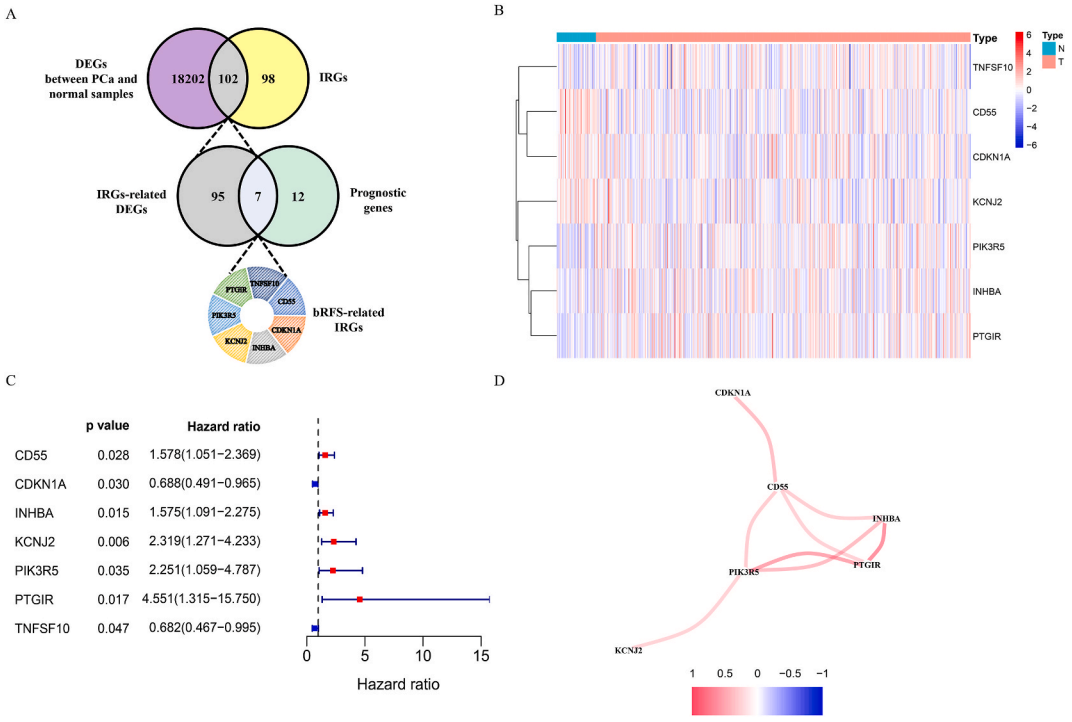

Fig. 2. Determination of the prognostic IRGs in the TCGA cohort. (A) Venn diagram for the analysis of the bRFS-related IRGs. **(B)** Heatmap displaying the expression changes and clustering relationship of 7 hub genes between PCa and normal samples (https://postimg.cc/WDcmYY3J). **(C)** Forest diagram displaying results of the univariate Cox regression analysis between 7 hub genes and bRFS. **(D)** Protein-protein interaction network indicating the correlation among prognostic IRGs. DEGs, differentially expressed genes; IRGs, inflammation-related genes; bRFS, biochemical recurrence-free survival.

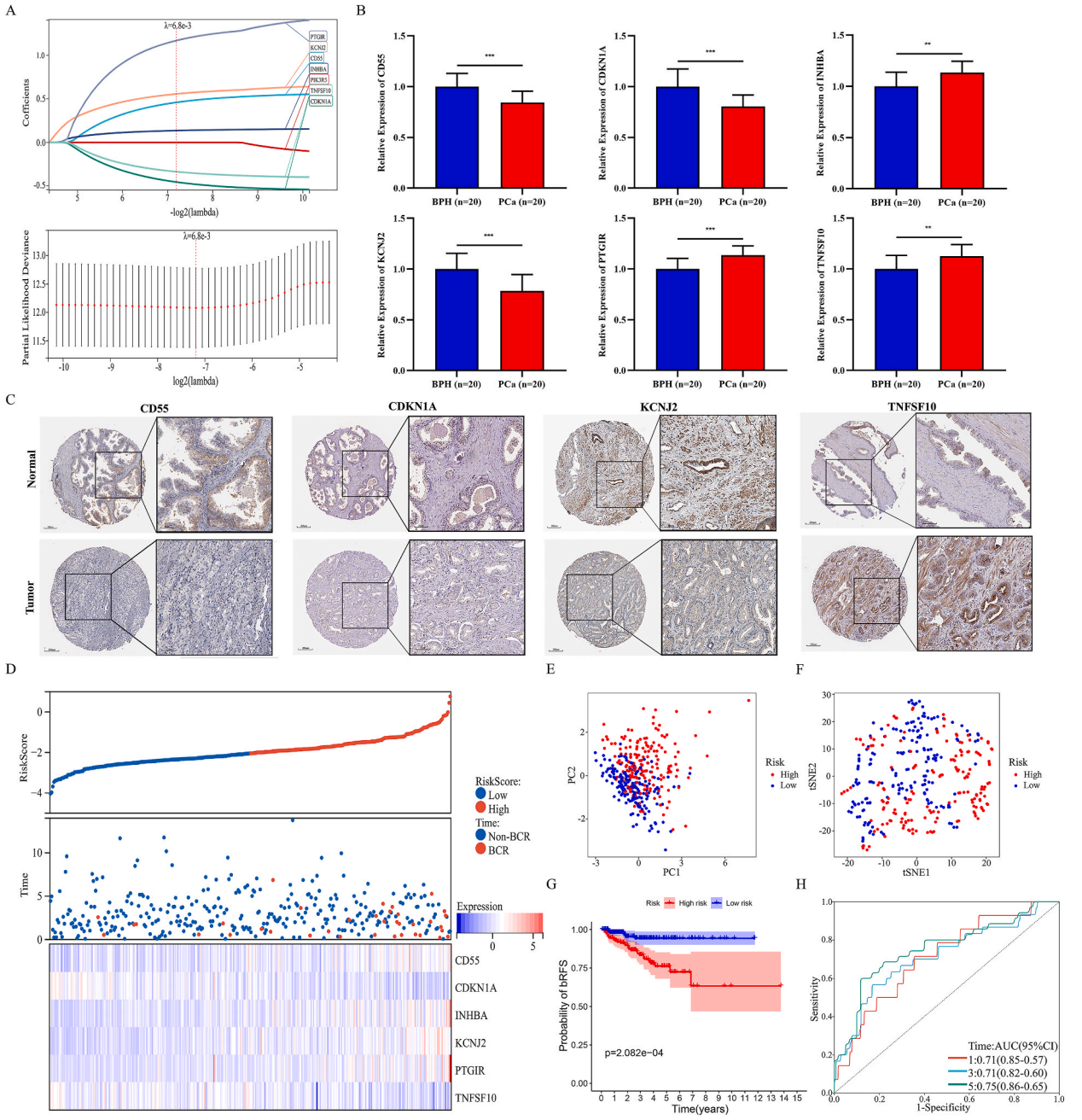

Fig. 3. Establishment of a novel IRPS in the TCGA cohort. (A) Coefficient curve and partial likelihood deviance of different quantitative variables. **(B)** Detection of mRNA levels for the model genes using RT-qPCR. **(C)** Assessment of protein levels for the model genes using data from the Human Protein Atlas. **(D)** The association between the risk score and follow-up time, outcomes, and alterations in the expression of model genes in PCa samples (https://postimg.cc/w7FSpJJv). **(E)** PCA plot. **(F)** t-SNE plot. **(G)** Kaplan–Meier survival curves illustrating the probability of bRFS stratified by the IRPS-based risk score. **(H)** ROC curves evaluating predictive accuracy of IRPS for 1 year, 3 years, and 5 years bRFS. IRPS, inflammation-related prognostic signature; PCA, principal component analysis; t-SNE, t-distributed stochastic neighbor embedding; ROC, receiver operating characteristic; $^{**}P < 0.01$, $^{***}P < 0.001$.

genes by RT-qPCR, we determined that INHBA, PTGIR, and TNFSF10 had higher expression in PCa compared to BPH samples, whereas CD55, CDKN1A, and KCNJ2 had lower expression levels (Fig. 3B). The similar trends were observed in protein levels for CD55, CDKN1A, KCNJ2, and TNFSF10 by evaluating the Human Protein Atlas (Fig. 3C). Regrettably, there were no available IHC images for INHBA and PTGIR on the website. Finally, a prognostic signature based on 6-IRGs was constructed and dubbed IRPS. And the IRPS-based score was calculated by the following formula: risk score = (0.460 × CD55) + (−0.458 × CDKN1A) + (0.136 × INHBA) +

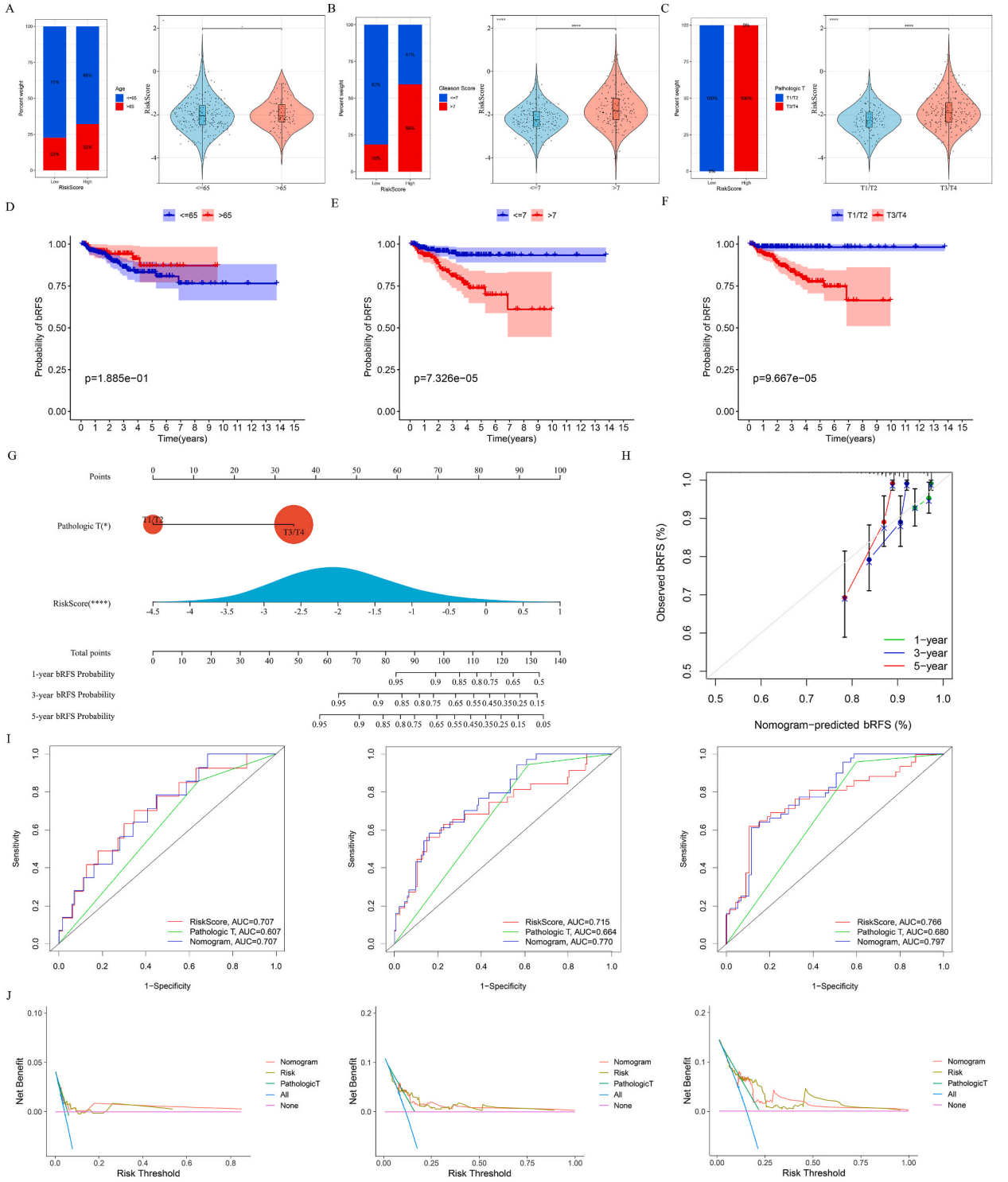

Fig. 4. Correlation between the IRPS and clinical characteristics in the TCGA cohort. (A–C) The proportion and the difference of age, Gleason score, and pathologic T stage in two groups. **(D–F)** Kaplan–Meier survival curves illustrating the probability of bRFS stratified by age, Gleason score, and pathologic T stage. **(G)** Nomogram combining risk score and pathologic T stage. **(H)** Calibration curves evaluating internal validation of nomogram for 1 year, 3 years, and 5 years bRFS. **(I)** ROC curves evaluating predictive accuracy of nomogram for 1 year, 3 years, and 5 years bRFS. **(J)** Decision curve analysis evaluating net benefit of nomogram for 1 year, 3 years, and 5 years bRFS. $^{****}P < 0.0001$.

(0.553 × KCNJ2) + (1.172 × PTGIR) + (−0.334 × TNFSF10).

Patients with PCa were classified into high- and low-risk groups based on the defined risk score cutoff. The risk score distribution and survival status indicated that the high-risk group exhibited a higher rate of BCR and a shorter bRFS time (Fig. 3D). PCA and t-SNE analysis revealed two tendencies in the distribution of samples in the two groups (Fig. 3E and F). Furthermore, Kaplan-Meier survival analysis demonstrated that patients in the low-risk group exhibited a more favorable survival prognosis (Fig. 3G). Consistently, the values of the areas under the curve (AUC) for 1-year, 3-year, and 5-year bRFS were 0.71, 0.71, and 0.75, respectively (Fig. 3H), indicating the excellent predictive power of the IRPS.

To validate the robustness of the TCGA cohort signature, two other external validation cohorts (MSKCC and GSE70769) were similarly classified as low- and high-risk groups using the same formula as the TCGA cohort (Figs. S1A and B). For the MSKCC cohort, PCA and t-SNE analysis confirmed that high- and low-risk groups were distributed in discrete directions (Figs. S1C and D). Likewise, the high-risk group exhibited a higher BCR probability compared to the low-risk group (Fig. S1G). Meanwhile, the AUCs for IRPS were 0.81 at 1 year, 0.68 at 3 years, and 0.72 at 5 years (Fig. S1I). For the GSE70769 cohort, same analyses were performed and similar findings were obtained (Figs. S1E, F, H and J).

3.3. Associations between IRPS and clinicopathological characteristics

To investigate the connection between clinicopathological factors and IRPS, we initially evaluated the disparity in IRPS between the two groups based on their clinicopathological characteristics. The scatter plots indicated that patients with advanced Gleason score and pathologic T stage exhibited higher risk score, whereas no significant age-related difference was observed in the TCGA cohort (Fig. 4A–C). In the MSKCC cohort, the same substantial difference in Gleason score was observed as in the TCGA cohort, but no difference among patients stratified by age and pathologic T stage (Figs. S2A–C). More interestingly, patients with advanced pathologic T stage in both the TCGA and MSKCC cohorts were consistently classified into the high-risk group (Fig. 4C and Fig. S2C). Through stratified survival analysis, we discovered that worse outcomes in patients with higher Gleason score (Fig. 4E and Fig. S2E) and pathologic T stage (Fig. 4F and Fig. S2F) in both the TCGA and MSKCC cohorts, despite no significant difference in age (Fig. 4D and Fig. S2D).

Next, univariate and multivariate Cox regression analyses were performed to evaluate the independence of IRPS in conjunction with clinicopathological factors. In the univariate Cox regression analysis, the pathologic T stage, Gleason score, and the IRPS-based score exhibited significantly associated with bRFS in both the TCGA and MSKCC cohorts (TCGA cohort: HR = 4.069, $P < 0.001$; HR = 10.040, $P < 0.05$; HR = 3.240, $P < 0.001$, respectively; MSKCC cohort: HR = 4.159, $P < 0.001$; HR = 4.379, $P < 0.001$; HR = 259.591, $P < 0.001$, respectively). In the multivariable Cox regression analysis, both the risk score and pathologic T stage were still proved to be independent predictors of bRFS (TCGA cohort: HR = 5.310, $P < 0.05$; HR = 2.207, $P < 0.001$, respectively; MSKCC cohort: HR = 3.773, $P < 0.001$; HR = 75.156, $P < 0.05$, respectively) (Table 2).

3.4. Construction and verification of the prognostic prediction nomogram

To assess the clinical utility of the IRPS, we constructed a nomogram with risk score and pathologic T stage in both the TCGA and MSKCC cohorts (Fig. 4G and Fig. S2G). Moreover, the calibration plots consistently demonstrated outstanding predictive accuracy in both the TCGA and MSKCC cohorts (Fig. 4H and Fig. S2H). Correspondingly, the AUCs of the nomogram in both cohorts suggested that the nomogram was superior to the risk score or pathologic T stage alone for predicting bRFS (Fig. 4I and Fig. S2I), and the nomogram consistently exhibited a higher net benefit compared to other characteristics in both cohorts (Fig. 4J and Fig. S2J).

3.5. Functional enrichment based on IRPS

To gain insights into the potential biological functions influenced by IRPS in PCa, 126 DEGs between the two risk groups were identified in the TCGA cohort. As we expected, the results of the GO analysis revealed enrichment for biological processes and molecular functions related to inflammation, including antigen binding and CXCR chemokine receptor binding (Fig. 5A–C). Additionally,

Table 2
Univariate and multivariate Cox regression analysis of clinical factors and IRPS in the TCGA cohort and the MSKCC cohort.

Variable	TCGA cohort				MSKCC cohort			
	Univariate		Multivariate		Univariate		Multivariate	
	HR	*P*	HR	*P*	HR	*P*	HR	*P*
Age (years) ≤65 vs > 65	0.580	0.194	0.503	0.106	1.489	0.382	1.049	0.918
Gleason score ≤7 vs >7	4.069	<0.001	2.005	0.094	4.159	<0.001	2.134	0.114
Pathologic T stage 1/2 vs 3/4	10.040	<0.05	5.310	<0.05	4.379	<0.001	3.733	<0.001
Risk score Low vs High	3.240	<0.001	2.207	<0.001	259.591	<0.001	75.156	<0.05

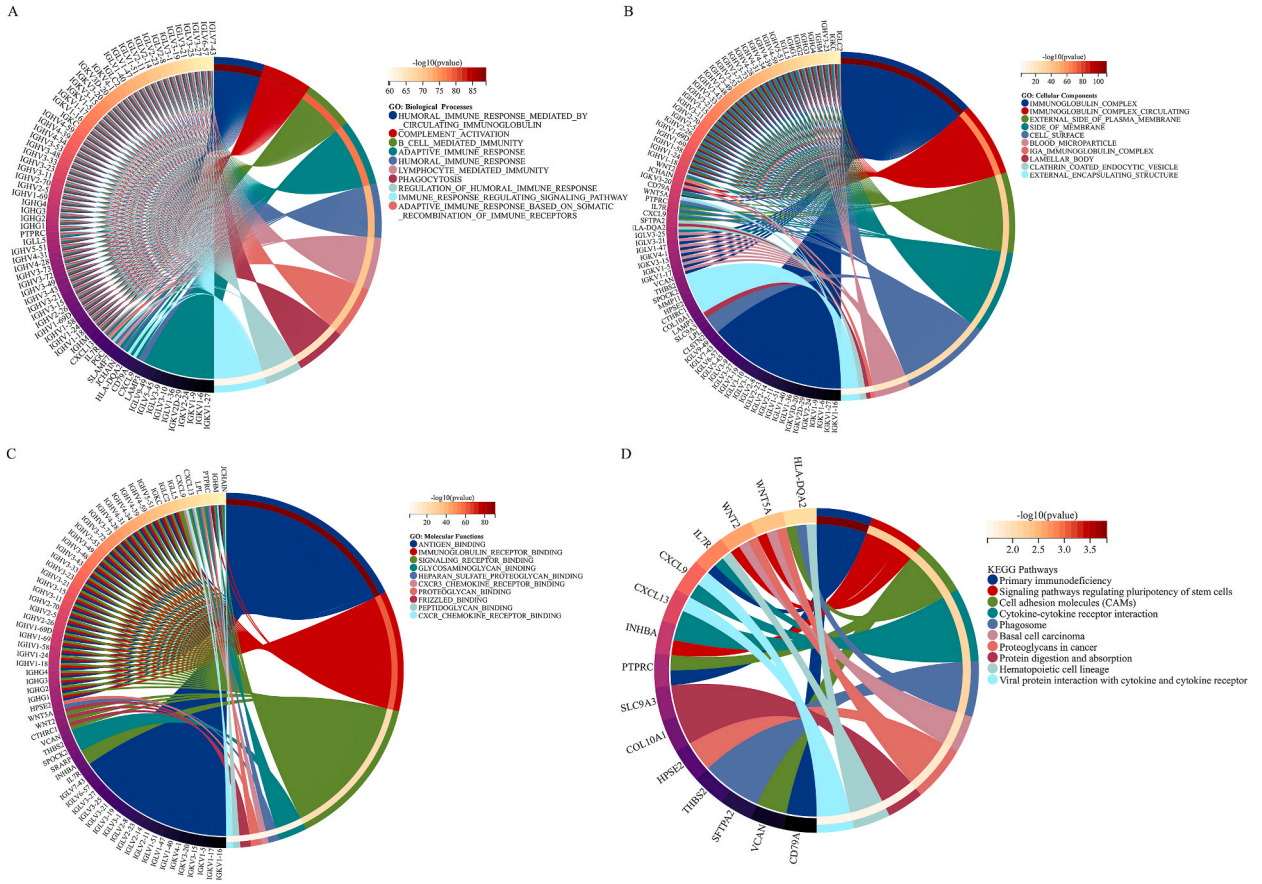

Fig. 5. Functional enrichment analysis of DEGs between risk groups in the TCGA cohort. (A–C) GO enrichment analysis for biological processes **(A)**, cellular components **(B)**, and molecular functions **(C)**. **(D)** KEGG pathways enrichment analysis. GO, gene ontology; KEGG, kyoto encyclopedia of genes and genomes.

KEGG pathway analysis also showed significant enrichment for cytokine-cytokine receptor interaction and primary immunodeficiency pathways (Fig. 5D). These data suggested that the difference in BCR-free survival across subgroups may be related to immunity.

3.6. Immune landscape based on IRPS

To delve deeper into the investigation and verify the association between the IRPS and the tumor immunity in PCa samples, we initially studied the distribution of IRPS-based genes in immune cells of PCa at the single-cell sequencing level. A total of 14 cell clusters composed of 15156 cells were finally identified, including T cells, monocytes, pre-B cell $CD34^{-}$, granulocyte-monocyte progenitor, chondrocytes, endothelial cells, pre-B cell $CD34^{+}$, tissue stem cells, common myeloid progenitor, epithelial cells, megakaryocyte erythroid progenitor, B cells, macrophage, and natural killer cells (Fig. 6A). Unlike CD55 and CDKN1A, which were highly expressed in a variety of immune cells, it was discovered that INHBA, KCNJ2, PTGIR, and TNFSF10 were expressed with some specificity in immune cells (Fig. 6B–D), suggesting that these genes may play a role in regulating specific immune cells and that IRPS has an immune predictive value at the single cell level.

Subsequently, the heatmap and correlation coefficients were generated to visualize the associations between immune cell types and risk score calculated using 7 algorithms based on the IRPS (Fig. 7A and B). In addition, we discovered that patients in the high-risk subgroup exhibited significantly higher immune and stromal scores, while their tumor purity was lower compared to the low-risk subgroup (Fig. 7C), suggesting greater immune cell infiltration and immune molecule presence in PCa tissues from the high-risk IRPS subgroup. Notably, the high-risk group exhibited much higher scores for 12/16 immune cell types and 11/13 immune-related processes (Fig. 7D and E). Further analysis revealed differences between risk groups at certain steps of the cancer immune cycle (Fig. 7F). Together, these findings showed the distinctive tumor immunogram in PCa, providing new insights into the underlying mechanisms of IRPS.

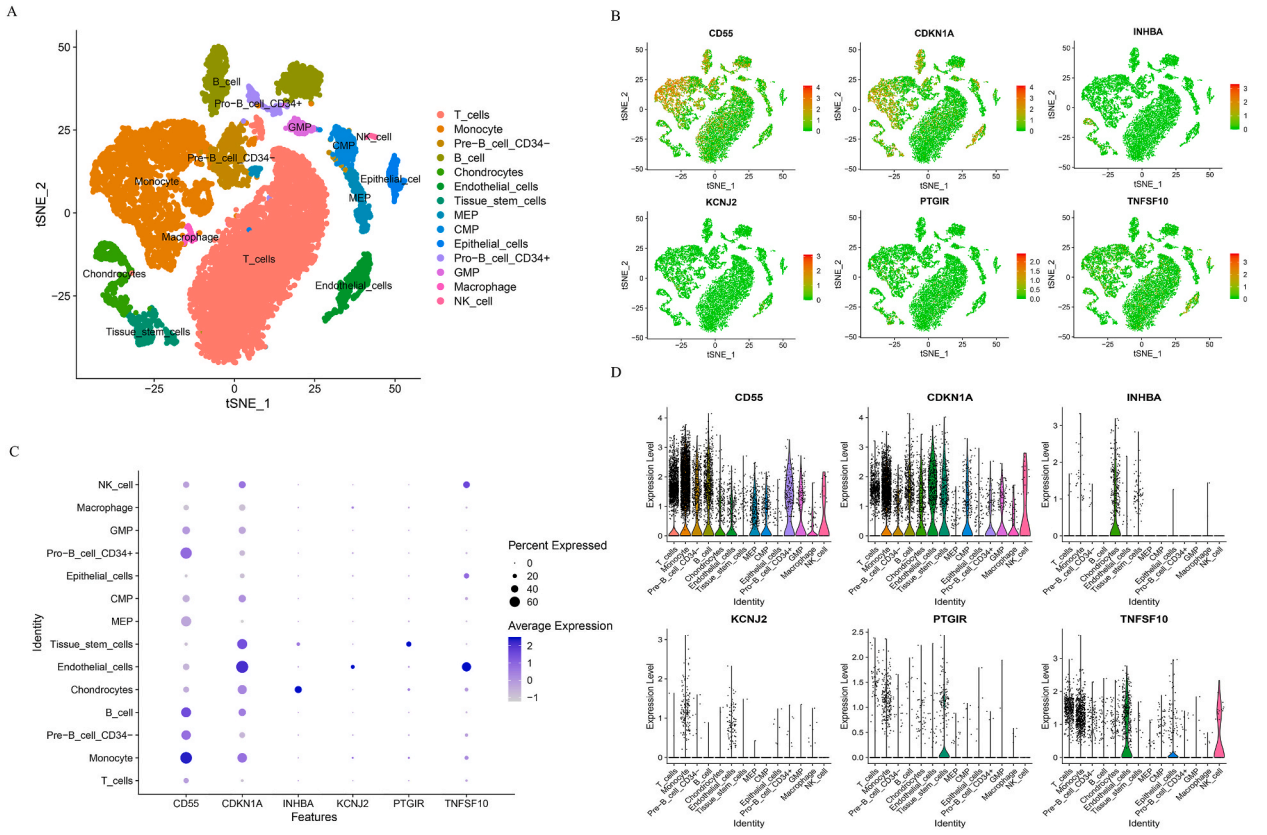

Fig. 6. The role of the IRPS at the single-cell sequencing level. (A) t-SNE plot based on the manually annotated cell, with distinct colors denoting various cell groups. **(B–D)** t-SNE plots **(B)**, bubble plots **(C)**, and violin plots **(D)** displaying the distribution of the IRPS-based genes in immune cells. MEP, megakaryocyte erythroid progenitor; CMP, common myeloid progenitor; GMP, granulocyte-monocyte progenitor.

3.7. Genomic heterogeneity and immunotherapeutic responses based on IRPS

Considering the substantial impact of tumor heterogeneity on the immune microenvironment [45], we conducted a comprehensive exploration of key tumor heterogeneity features based on the IRPS, including HDR, LOH, MATH, MSI, neoantigen, ploidy, TMB, CNV, and epigenetic modification. Our observations revealed a significantly higher frequency of CNV in the high-risk group compared to the low-risk group (Fig. 8A). Among IRPS-based genes, INHBA, TNFSF10, and CD55 exhibited comparatively high amplification, while KCNJ2, CDKN1A, and PTGIR primarily displayed deletion events (Fig. 8B and C). Interestingly, while TMB alone did not significantly affect survival, a combined effect of TMB and IRPS on BCR outcome was observed in patients with PCa, such that a high-risk score and a high TMB were associated with a shorter time to BCR (Fig. 8D–F). We also analyzed the mutation data to further understand the molecular factors of different subsets. The results indicated that PCa patients in the high-risk group exhibited a higher number of mutations than those in the low-risk group. Interestingly, missense mutations were the predominant mutation type in two risk groups, with mutation rates exceeding 10 % for TP53, TTN, and SPOP in both groups (Fig. 8G). Furthermore, 24/43 epigenetic modification genes significantly correlated with the IRPS (Fig. 8H). Additionally, we found that the risk score positively correlated with HRD ($R = 0.27$, $P < 0.001$), LOH ($R = 0.25$, $P < 0.001$), MSI ($R = 0.14$, $P < 0.01$), and ploidy ($R = 0.16$, $P < 0.01$) but not with MATH and neoantigen (Fig. 8I). These findings underscore the potential utility of IRPS in exploring the heterogeneity of PCa.

Given the crucial influence of immune checkpoints on therapeutic outcomes and immune responses, we found that 37/46 immune checkpoints, including CTLA4 and PDCD1, exhibited a significant positive association with IRPS, while TNFSF9 displayed a notable negative correlation ($P < 0.05$) (Fig. S3A). Moreover, we performed a specific computation of the immunophenoscore for patients undergoing various treatments, indicating that individuals with a low risk score might demonstrate heightened sensitivity to immunotherapy targeting CTLA4 negative/PD1 negative pathways, potentially achieving more favorable therapeutic responses (Fig. S3B).

3.8. Pharmaceutical analysis based on IRPS

To investigate the potential utility of IRPS in the context of precise treatment of PCa, we analyzed the sensitivity of 6 commonly used anticancer drugs, including bicalutamide, cisplatin, docetaxel, gemcitabine, paclitaxel, and doxorubicin, between the two groups.

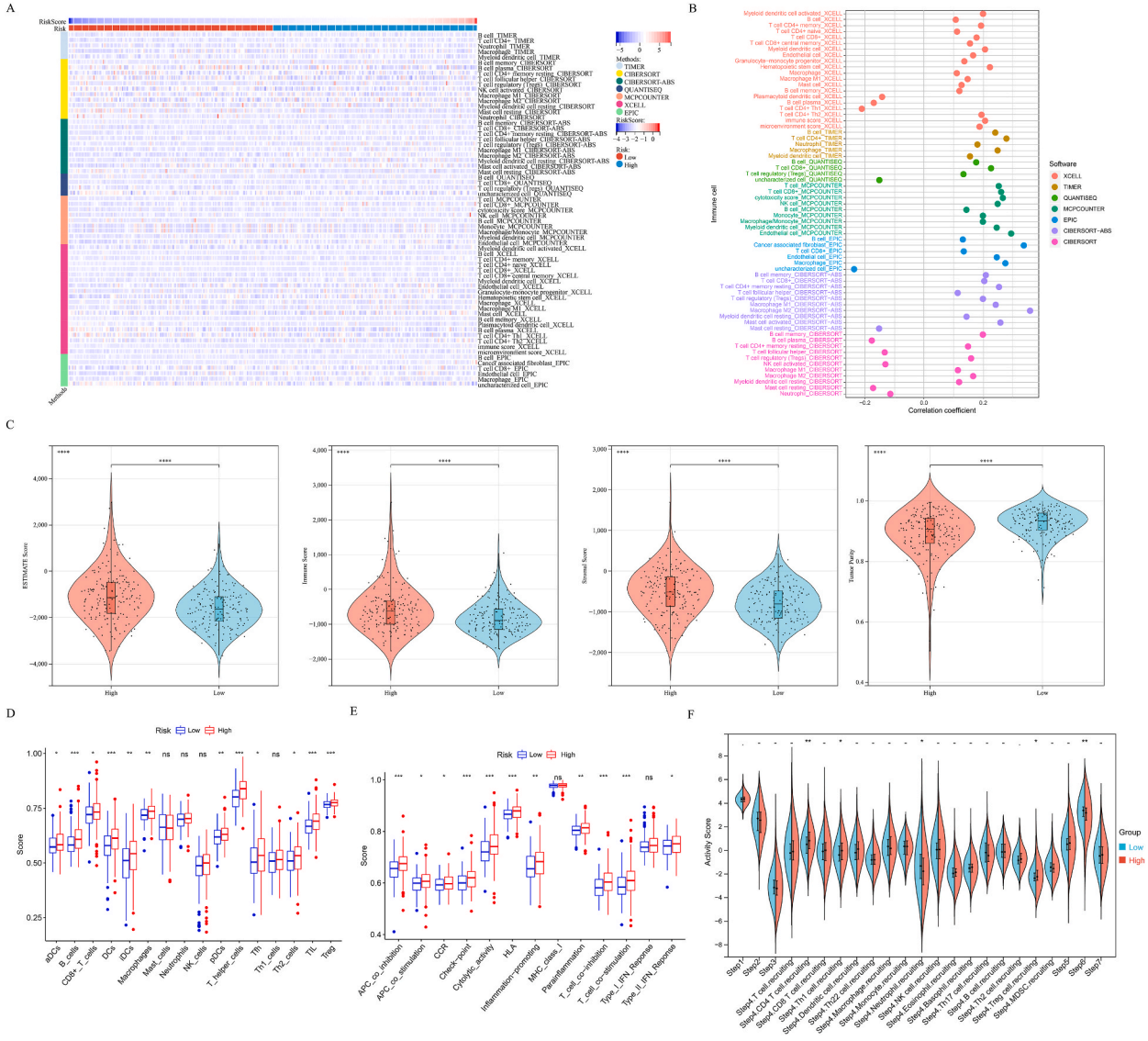

Fig. 7. Association between the IRPS and immune landscape in PCa. (A) Heatmap showing estimated tumor-infiltrating immune cells by seven algorithms in risk groups. **(B)** Lollipop plot depicting correlation coefficients between immune cell infiltration and risk score using seven algorithms. **(C)** Difference in the assessment indices of tumor microenvironment between risk groups. **(D)** Difference in the 16 cells about immunity between risk groups. **(E)** Difference in the 13 functions about immunity between risk groups. **(F)** Difference in activity scores for steps of the cancer-immunity cycle between risk groups; $^{*}P < 0.05$, $^{**}P < 0.01$, $^{***}P < 0.001$, $^{****}P < 0.0001$. ns, not significant.

Drug sensitivity results demonstrated that bicalutamide and docetaxel were more likely to play a drug role in patients in the high-risk group, but low-risk patients were more sensitive to gemcitabine, cisplatin, and paclitaxel (Fig. 9A). On the basis of targeted pharmacological therapy, we compared and assessed the expression of targeted genes downloaded from the DrugBank database in two groups (Fig. 9B). The preceding findings revealed that IRPS could assist doctors in making better tailored medicine selections and assist patients in making better treatment decisions.

To evaluate the binding affinities between IRPS proteins and drugs, we docked the 5 drugs with IRPS-based proteins. The minimum binding energy for each interaction was calculated. 15/24 drug-gene pairs had minimum binding energies < -6.0 kcal/mol, except cisplatin which could not be successfully docked (Fig. 9C), suggesting stable binding for most pairs. At the same time, we found that except for cisplatin could not be docked, the other 4 drugs (bicalutamide, docetaxel, gemcitabine, and paclitaxel) had a higher affinity with PTGIR (Fig. 9D–G), suggesting that these drugs were likely to play a certain biological effect on PTGIR.

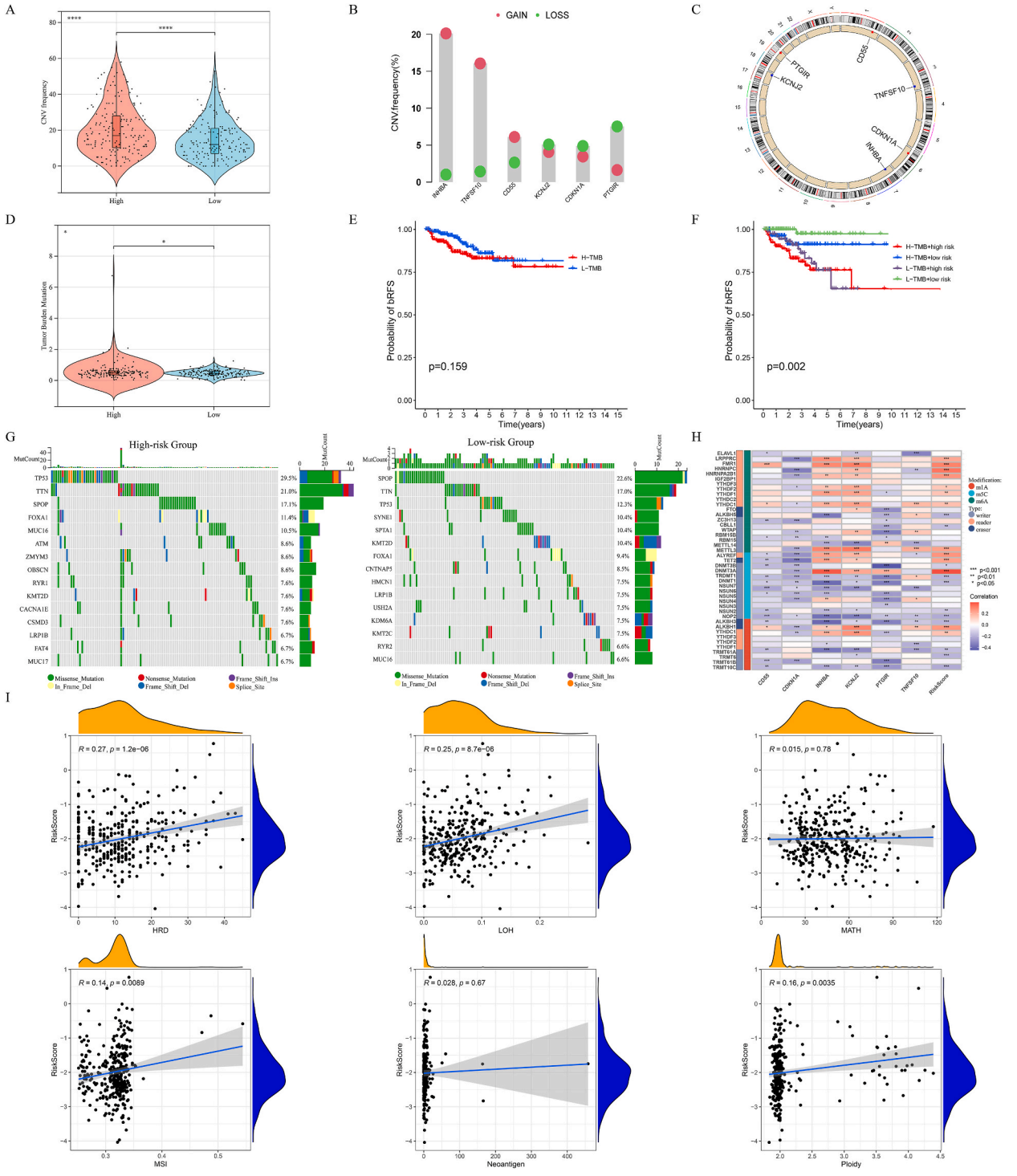

Fig. 8. Genomic heterogeneity based on IRPS. (A) Comparison of CNV frequency between risk groups. **(B)** CNV frequency (%) of the 6 model genes. **(C)** Localization of CNV events within the model genes on the chromosome. **(D)** Comparative analysis of TMB between risk groups. **(E and F)** Kaplan–Meier survival curves illustrating the probability of bRFS stratified by TMB or IRPS-based risk score with TMB. **(G)** Waterfall plot of gene mutations in risk groups. **(H and I)** Relationship between risk score and several genomic features, including RNA-modified genes, HDR, LOH, MATH, MSI, Neoantigen, and Ploidy. CNV, copy number variation; TMB, tumor mutational burden; HRD, homologous recombination defect; LOH, loss of heterozygosity; MATH, mutant-allele tumor heterogeneity; MSI, microsatellite instability; $^{*}P < 0.05$, $^{****}P < 0.0001$.

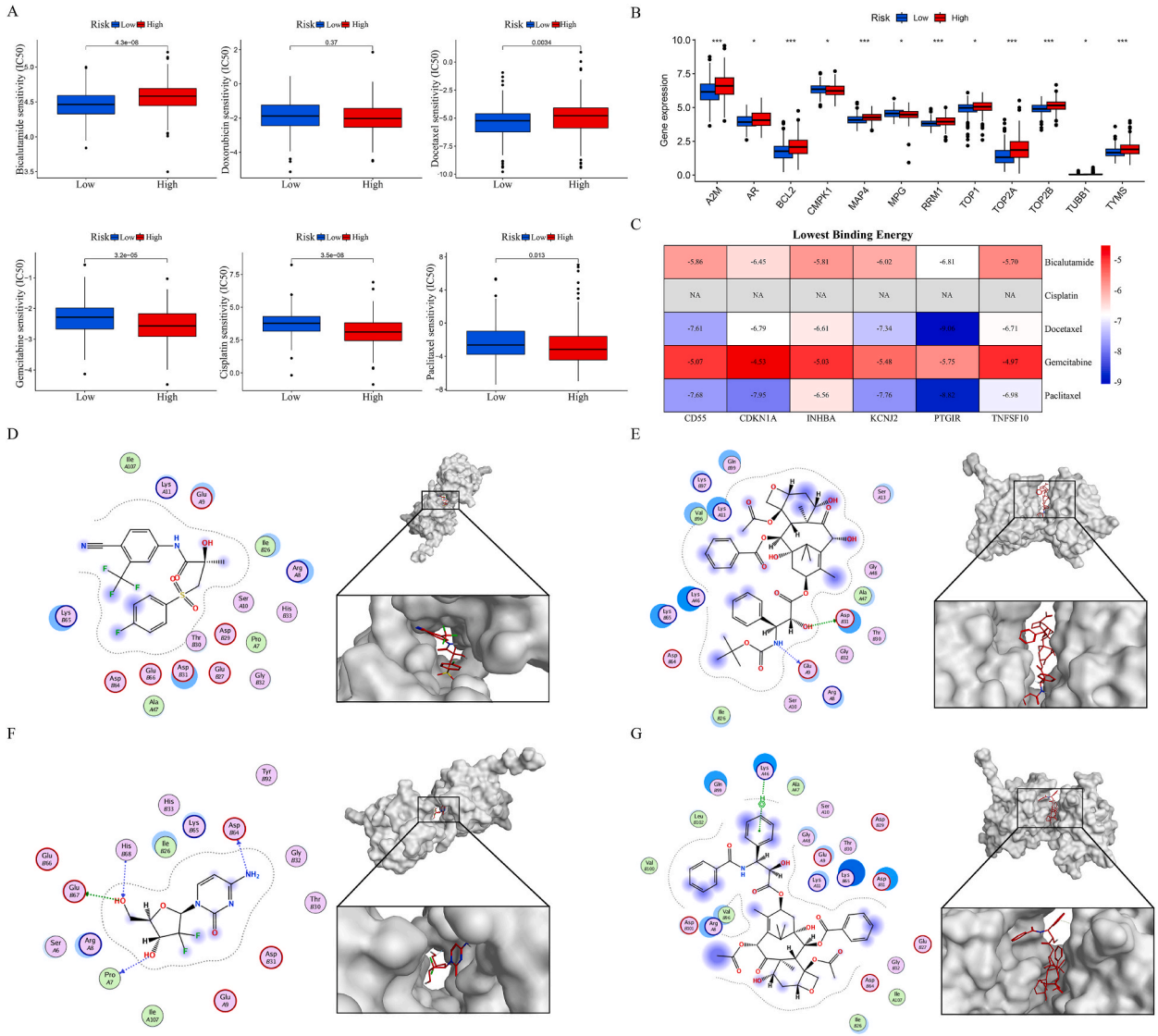

Fig. 9. Assessment of drug therapy by the IRPS. (A) Drug sensitivity of bicalutamide, gemcitabine, doxorubicin, cisplatin, docetaxel, and paclitaxel between risk groups in PCa patients. **(B)** Discrepancy in expression of target genes in anticancer drugs between risk groups. **(C)** Heat map displaying lowest binding energy of molecular docking. **(D–G)** 2D (left images) or 3D (right images) binding modes of Bicalutamide-PTGIR **(D)**, Docetaxel-PTGIR **(E)**, Gemcitabine-PTGIR **(F)**, and Paclitaxel-PTGIR **(G)**. $^{*}P < 0.05$, $^{***}P < 0.001$.

4. Discussion

Evidence has accumulated that inflammation and cancer are tightly correlated, not only revealing inflammatory factors and immune cells as predictive factors but also revealing their relationship with poor outcomes [46–48]. Cancer-associated inflammation, whether inherent to the cancer or induced by it, can create an immunosuppressive TME that promotes tumor development. In cases where an inflammatory TME has already been established, inflammatory factors may activate oncogenes and subsequently inactivate tumor suppressor genes, leading to increased cell proliferation and prolonged cell survival [49]. In addition, earlier research indicates that inflammatory response-related indicators are highly accurate at predicting the prognosis of some malignancies, including gastric cancer [50] and colon cancer [51]. Inflammation of the prostate is known to plays a role in the etiology and progression of PCa [52]. Therefore, the construction of IRPS is of great significance for predicting survival outcomes and exploring new therapeutic strategies for PCa patients. To the best of our knowledge, this represents the inaugural report on the IRPS for prognostication, tumor microenvironment, and drug choices in PCa.

In this study, we systematically investigated inflammation-related genes with predictive significance in PCa and their correlation with bRFS. In addition, using the LASSO-Cox regression approach, we established that IRPS was composed of 6 genes, including CD55, CDKN1A, INHBA, KCNJ2, PTGIR, and TNFSF10. Furthermore, we determined the expression levels of these genes in PCa using RT-

qPCR and IHC. Previous reports have indeed highlighted the pivotal roles of these six model genes in both inflammation and cancer [53–61]. Although these reports reported the relationship between a single inflammation-related gene and cancer, it is necessary to explore a comprehensive model with enhanced prognostic predictive capabilities. In both the training and validation cohorts of our study, both IRPS and the nomogram by pathologic T stage plus risk score based on IRPS performed well.

Despite the fact that PCa, an immune-responsive illness, is regarded as an ideal tumor model for immunotherapy [62], the potential regulation between tumor immune and inflammation remains unknown. According to the GO and KEGG analysis, we unexpectedly observed that the results implicated numerous biological processes and pathways about immunity. Therefore, we boldly speculated that inflammation might be closely related to tumor immunity in PCa. Regrettably, the relationship between tumor inflammation and the tumor immune microenvironment in PCa has been relatively underexplored in detail. As we expected, we initially found differences in the distribution of IRPS-based genes in immune cell types through scRNA-seq analysis. There were also substantial variations in the infiltration patterns of immune-related cells and functions within the two distinct IRPS-based groups. Immunosuppressive cells, such as pCDs and Tregs, were associated with a higher risk score, which may indicate a bad prognosis for patients in the high-risk group. Meanwhile, our findings demonstrated that PCa patients with a higher TMB combined risk score had a poorer prognosis, which was similar to the previous findings [63]. High-TMB is widely regarded as a promising biomarker for predicting the response to immune checkpoint inhibition therapy for multiple cancers, however, McGrail demonstrates that TMB does not show satisfactory predictive accuracy for the response to ICI in PCa patients [64]. Given the above, it may explain why TMB did not show a significant difference in predicting the survival outcomes of PCa patients alone.

CTLA4 and PD1 are the most common targets for immune checkpoint inhibition therapy [65], and we observed that PCa patients in the low-risk group had higher sensitivity to CTLA4 negative/PD1 negative immunotherapy. In addition, patients with varying risk score may respond differentially to antineoplastic drugs (bicalutamide, docetaxel, gemcitabine, cisplatin, and paclitaxel), and target genes, such as A2M, BCL2, MAP4, RRM1, and TYMS, also differed significantly among subgroups. More interestingly, PTGIR showed a strong affinity for a variety of antineoplastic drugs, which is worth thinking about whether it has the opportunity to become a marker for drug selection. As described above, these findings suggest that the risk score derived from the IRPS is of clinical significance in predicting the survival status of PCa patients. The signature will be a reliable model for evaluating the efficiency of chemotherapy and immunotherapy, and providing drug choices for clinical treatment.

Notwithstanding the intriguing discoveries within this study, it is imperative to acknowledge several inherent limitations. Firstly, the samples were obtained from the public database, so prospective studies on a larger population of patients are crucial for the clinical application of IRPS in PCa patients. Secondly, although we have performed some of the basic experiments, such as RT-qPCR, it is undeniable that more comprehensive functional experiments are needed to confirm their effect on PCa. Finally, deeper clinical trials are necessary to validate the correlation between our prognostic signature and immune landscape as well as our response to antitumor drugs.

5. Conclusions

In summary, we have developed a novel IRPS that is of satisfactory accuracy in prognosticating the outcomes and therapeutic responses in PCa. Therefore, the signature will not only hold promise as a robust biomarker for predicting bRFS and immune profile characteristics, but also offer a promising avenue for redefining treatment strategies and drug selection in the management of PCa patients.

Author contribution statement

Weian Zhu: conceived and designed the experiments, performed the experiments, analyzed and interpreted the data, wrote the paper.

Jiongduan Huang and Jianjie Wu: analyzed and interpreted the data, wrote the paper.

Chenglun Wu, Fengxi Ye and Xiang Li: contributed reagents, materials, analysis tools or data.

Wenjie Lai: performed the experiments, wrote the paper.

Data availability statement

Data included in article/supplementary material/referenced in article.

Supplementary content related to this article has been published online at [URL].

Ethics statement

The studies involving human participants have been performed in accordance with the Declaration of Helsinki. All the selected samples were informed consent of the patients and approved by the Clinical Ethics Board of the Third Affiliated Hospital of Sun Yat-sen University (No. 2020-02-105).

Funding statement

This work was supported by the National Natural Science Foundation of China [grant numbers: 82303906] and the Basic and

Applied Basic Research Foundation of Guangdong Province [grant numbers: 2021A1515111210, 2023A1515010588].

Declaration of competing interest

The authors declare that they have no known competing financial interests or personal relationships that could have appeared to influence the work reported in this paper.

Appendix A. Supplementary data

Supplementary data to this article can be found online at https://doi.org/10.1016/j.heliyon.2023.e21174.

References

[1] M.B. Culp, et al., Recent global patterns in prostate cancer incidence and mortality rates, Eur. Urol. 77 (1) (2020) 38–52, https://doi.org/10.1016/j.eururo.2019.08.005.
[2] R.L. Siegel, et al., Cancer statistics, 2022, CA, Cancer J. Clin. 72 (1) (2022), https://doi.org/10.3322/caac.21708, 7–33.
[3] K. Komura, et al., Current treatment strategies for advanced prostate cancer, Int. J. Urol. 25 (3) (2018) 220–231, https://doi.org/10.1111/iju.13512.
[4] J.A. Brockman, et al., Nomogram predicting prostate cancer-specific mortality for men with biochemical recurrence after radical prostatectomy, Eur. Urol. 67 (6) (2015) 1160–1167, https://doi.org/10.1016/j.eururo.2014.09.019.
[5] P. Cornford, et al., EAU-ESTRO-SIOG guidelines on prostate cancer. part II: treatment of relapsing, metastatic, and castration-resistant prostate cancer, Eur. Urol. 71 (4) (2017) 630–642, https://doi.org/10.1016/j.eururo.2016.08.002.
[6] A. Mantovani, et al., Cancer-related inflammation, Nature 454 (7203) (2008) 436–444, https://doi.org/10.1038/nature07205.
[7] A. Ben-Baruch, Inflammation-associated immune suppression in cancer: the roles played by cytokines, chemokines and additional mediators, Semin. Cancer Biol. 16 (1) (2006) 38–52, https://doi.org/10.1016/j.semcancer.2005.07.006.
[8] F. Colotta, et al., Cancer-related inflammation, the seventh hallmark of cancer: links to genetic instability, Carcinogenesis 30 (7) (2019) 1073–1081, https://doi.org/10.1093/carcin/bgp127.
[9] A. Rani, et al., Prostate cancer: the role of inflammation and chemokines, Am. J. Pathol. 189 (11) (2019) 2119–2137, https://doi.org/10.1016/j.ajpath.2019.07.007.
[10] T. Cai, et al., Current knowledge of the potential links between inflammation and prostate cancer, Int. J. Mol. Sci. 20 (15) (2019) 3833, https://doi.org/10.3390/ijms20153833.
[11] F. Sessa, et al., Inflammation and prostate cancer: pathological analysis from pros-IT CNR 2, Cancers 15 (3) (2023) 630, https://doi.org/10.3390/cancers15030630.
[12] M.R. Junttila, F.J. de Sauvage, Influence of tumour micro-environment heterogeneity on therapeutic response, Nature 501 (7467) (2013) 346–354, https://doi.org/10.1038/nature12626.
[13] D. Denk, F.R. Greten, Inflammation: the incubator of the tumor microenvironment, Trends Cancer 8 (11) (2022) 901–914, https://doi.org/10.1016/j.trecan.2022.07.002.
[14] J.S. de Bono, et al., Prostate carcinogenesis: inflammatory storms, Nat. Rev. Cancer 20 (8) (2020) 455–469, https://doi.org/10.1038/s41568-020-0267-9.
[15] Y. Zhang, Z. Zhang, The history and advances in cancer immunotherapy: understanding the characteristics of tumor-infiltrating immune cells and their therapeutic implications, Cell, Mol. Immunol. 17 (8) (2020) 807–821, https://doi.org/10.1038/s41423-020-0488-6.
[16] H. Zhang, et al., Machine learning-based tumor-infiltrating immune cell-associated lncRNAs for predicting prognosis and immunotherapy response in patients with glioblastoma, Brief Bioinform 23 (6) (2022) bbac386, https://doi.org/10.1093/bib/bbac386.
[17] N. Zhang, et al., Machine learning-based identification of tumor-infiltrating immune cell-associated lncRNAs for improving outcomes and immunotherapy responses in patients with low-grade glioma, Theranostics 12 (13) (2022) 5931–5948, https://doi.org/10.7150/thno.74281.
[18] S. Chen, et al., Single-cell analysis reveals transcriptomic remodellings in distinct cell types that contribute to human prostate cancer progression, Nat. Cell Biol. 23 (1) (2021) 87–98, https://doi.org/10.1038/s41556-020-00613-6.
[19] H. Song, et al., Single-cell analysis of human primary prostate cancer reveals the heterogeneity of tumor-associated epithelial cell states, Nat. Commun. 13 (1) (2022) 141, https://doi.org/10.1038/s41467-021-27322-4.
[20] G. Ge, et al., Single-cell RNA-seq reveals a developmental hierarchy super-imposed over subclonal evolution in the cellular ecosystem of prostate cancer, Adv. Sci. 9 (15) (2022), e2105530, https://doi.org/10.1002/advs.202105530.
[21] A. Colaprico, et al., TCGAbiolinks: an R/Bioconductor package for integrative analysis of TCGA data, Nucleic Acids Res. 44 (8) (2016) e71, https://doi.org/10.1093/nar/gkv1507.
[22] A. Zehir, et al., Mutational landscape of metastatic cancer revealed from prospective clinical sequencing of 10,000 patients, Nat. Med. 23 (6) (2017) 703–713, https://doi.org/10.1038/nm.4333.
[23] H. Ross-Adams, et al., Integration of copy number and transcriptomics provides risk stratification in prostate cancer: a discovery and validation cohort study, EBioMedicine 2 (9) (2015) 1133–1144, https://doi.org/10.1016/j.ebiom.2015.07.017.
[24] A. Liberzon, et al., The Molecular Signatures Database (MSigDB) hallmark gene set collection, Cell Syst 1 (6) (2015) 417–425, https://doi.org/10.1016/j.cels.2015.12.004.
[25] D. Szklarczyk, et al., STRING v11: protein-protein association networks with increased coverage, supporting functional discovery in genome-wide experimental datasets, Nucleic Acids Res. 47 (D1) (2019) D607–D613, https://doi.org/10.1093/nar/gky1131.
[26] P. Shannon, et al., Cytoscape: a software environment for integrated models of biomolecular interaction networks, Genome Res. 13 (11) (2003) 2498–2504, https://doi.org/10.1101/gr.1239303.
[27] W. Zhu, et al., Multi-omics analysis reveals a macrophage-related marker gene signature for prognostic prediction, immune landscape, genomic heterogeneity, and drug choices in prostate cancer, Front. Immunol. 14 (2023), 1122670, https://doi.org/10.3389/fimmu.2023.1122670.
[28] A. Asplund, et al., Antibodies for profiling the human proteome-the human protein atlas as a resource for cancer research, Proteomics 12 (13) (2012) 2067–2077, https://doi.org/10.1002/pmic.201100504.
[29] Y. Liao, et al., WebGestalt 2019: gene set analysis toolkit with revamped UIs and APIs, Nucleic Acids Res. 47 (W1) (2019) W199, https://doi.org/10.1093/nar/gkz401. –W205.
[30] J. Racle, D. Gfeller, EPIC: a tool to estimate the proportions of different cell types from bulk gene expression data, Methods Mol. Biol. 2120 (2020) 233–248, https://doi.org/10.1007/978-1-0716-0327-7_17.
[31] D. Aran, et al., xCell: digitally portraying the tissue cellular heterogeneity landscape, Genome Biol. 18 (1) (2017) 220, https://doi.org/10.1186/s13059-017-1349-1.
[32] E. Becht, et al., Estimating the population abundance of tissue-infiltrating immune and stromal cell populations using gene expression, Genome Biol. 17 (1) (2016) 218, https://doi.org/10.1186/s13059-016-1070-5.

[33] F. Finotello, et al., Molecular and pharmacological modulators of the tumor immune contexture revealed by deconvolution of RNA-seq data, Genome Med. 11 (1) (2019) 34, https://doi.org/10.1186/s13073-019-0638-6.
[34] A.M. Newman, et al., Robust enumeration of cell subsets from tissue expression profiles, Nat. Methods 12 (5) (2015) 453–457, https://doi.org/10.1038/nmeth.3337.
[35] T. Li, et al., TIMER: a web server for comprehensive analysis of tumor-infiltrating immune cells, Cancer Res. 77 (21) (2017), https://doi.org/10.1158/0008-5472.CAN-17-0307 e108–e110.
[36] M.S. Rooney, et al., Molecular and genetic properties of tumors associated with local immune cytolytic activity, Cell 160 (1–2) (2015) 48–61, https://doi.org/10.1016/j.cell.2014.12.033.
[37] X. Chen, et al., Turning up the heat on non-immunoreactive tumors: pyroptosis influences the tumor immune microenvironment in bladder cancer, Oncogene 40 (45) (2021) 6381–6393, https://doi.org/10.1038/s41388-021-02024-9.
[38] C.H. Mermel, et al., GISTIC2.0 facilitates sensitive and confident localization of the targets of focal somatic copy-number alteration in human cancers, Genome Biol. 12 (4) (2011) R41, https://doi.org/10.1186/gb-2011-12-4-r41.
[39] V. Thorsson, et al., The immune landscape of cancer, Immunity 48 (4) (2018) 812–830.e14, https://doi.org/10.1016/j.immuni.2018.03.023.
[40] P. Charoentong, et al., Pan-cancer immunogenomic analyses reveal genotype-immunophenotype relationships and predictors of response to checkpoint blockade, Cell Rep. 18 (1) (2017) 248–262, https://doi.org/10.1016/j.celrep.2016.12.019.
[41] W. Yang, et al., Genomics of drug sensitivity in cancer (GDSC): a resource for therapeutic biomarker discovery in cancer cells, Nucleic Acids Res. 41 (2013) D955–D961, https://doi.org/10.1093/nar/gks1111.
[42] D.S. Wishart, et al., DrugBank 5.0: a major update to the DrugBank database for 2018, Nucleic Acids Res. 46 (D1) (2018) D1074–D1082, https://doi.org/10.1093/nar/gkx1037.
[43] P.W. Rose, et al., The RCSB protein data bank: integrative view of protein, gene and 3D structural information, Nucleic Acids Res. 45 (D1) (2017) D271–D281, https://doi.org/10.1093/nar/gkw1000.
[44] Y. Wang, et al., PubChem BioAssay: 2017 update, Nucleic Acids Res. 45 (D1) (2017) D955–D963, https://doi.org/10.1093/nar/gkw1118.
[45] R. Bonneville, et al., Landscape of microsatellite instability across 39 cancer types, JCO Precis Oncol. 2017 (2017), https://doi.org/10.1200/PO.17.00073. PO.17.00073.
[46] W. Ma, et al., Prognostic value of inflammatory biomarkers in gastric cancer patients and the construction of a predictive model, Dig. Surg. 36 (5) (2019) 433–442, https://doi.org/10.1159/000493432.
[47] M. Zengin, Local inflammatory response can predict clinical outcome in patients with curatively resected stage-IIB colon cancer: an advanced methodological study, Pathol. Oncol. Res. 26 (3) (2020) 1805–1816, https://doi.org/10.1007/s12253-019-00758-2.
[48] X. Wang, et al., A novel nomogram integrated with inflammation-based factors to predict the prognosis of gastric cancer patients, Adv. Ther. 37 (6) (2020) 2902–2915, https://doi.org/10.1007/s12325-020-01356-4.
[49] H. Zhao, et al., Inflammation and tumor progression: signaling pathways and targeted intervention, Signal Transduct. Targeted Ther. 6 (1) (2021) 263, https://doi.org/10.1038/s41392-021-00658-5.
[50] T.K. Furuya, et al., Association between polymorphisms in inflammatory response-related genes and the susceptibility, progression and prognosis of the diffuse histological subtype of gastric cancer, Genes 9 (12) (2018) 631, https://doi.org/10.3390/genes9120631.
[51] Y. Liang, et al., Identification and validation of a novel inflammatory response-related gene signature for the prognosis of colon cancer, J. Inflamm. Res. 14 (2021) 3809–3821, https://doi.org/10.2147/JIR.S321852.
[52] C.D. Nunzio, et al., The controversial relationship between benign prostatic hyperplasia and prostate cancer: the role of inflammation, Eur. Urol. 60 (1) (2011) 106–117, https://doi.org/10.1016/j.eururo.2011.03.055.
[53] R. Bharti, et al., CD55 in cancer: complementing functions in a non-canonical manner, Cancer Lett. 551 (2022), 215935, https://doi.org/10.1016/j.canlet.2022.215935.
[54] N.N. Kreis, et al., The multifaceted p21 (Cip1/Waf1/CDKN1A) in cell differentiation, migration and cancer therapy, Cancers 11 (9) (2019) 1220, https://doi.org/10.3390/cancers11091220.
[55] W. Lai, et al., HJURP promotes proliferation in prostate cancer cells through increasing CDKN1A degradation via the GSK3β/JNK signaling pathway, Cell Death Dis. 12 (6) (2021) 583, https://doi.org/10.1038/s41419-021-03870-x.
[56] M.A. Mouti, S. Pauklin, TGFB1/INHBA homodimer/Nodal-SMAD2/3 signaling network: a pivotal molecular target in PDAC treatment, Mol. Ther. 29 (3) (2021) 920–936, https://doi.org/10.1016/j.ymthe.2021.01.002.
[57] T. Si, et al., High expression of INHBA is an adverse prognostic factor for de novo acute myeloid leukemia, Leuk. Lymphoma 59 (1) (2018) 114–120, https://doi.org/10.1080/10428194.2017.1324157.
[58] C. Huang, et al., Interaction of the Ca2+-sensing receptor with the inwardly rectifying potassium channels Kir4.1 and Kir4.2 results in inhibition of channel function, Am. J. Physiol. Ren. Physiol. 292 (3) (2007) F1073–F1081, https://doi.org/10.1152/ajprenal.00269.2006.
[59] R. Vicente, et al., The systemic inflammatory response is involved in the regulation of K(+) channel expression in brain via TNF-alpha-dependent and -independent pathways, FEBS Lett. 572 (1–3) (2004) 189–194, https://doi.org/10.1016/j.febslet.2004.07.030.
[60] T. Kanazawa, et al., G-Protein-Coupled receptors: next generation therapeutic targets in head and neck cancer? Toxins 7 (8) (2015) 2959–2984, https://doi.org/10.3390/toxins7082959.
[61] Y.T. Oh, S.Y. Sun, Regulation of cancer metastasis by TRAIL/death receptor signaling, Biomolecules 11 (4) (2021) 499, https://doi.org/10.3390/biom11040499.
[62] C.G. Drake, Prostate cancer as a model for tumour immunotherapy, Nat. Rev. Immunol. 10 (8) (2010) 580–593, https://doi.org/10.1038/nri2817.
[63] C. Luo, J. Chen, L. Chen, Exploration of gene expression profiles and immune microenvironment between high and low tumor mutation burden groups in prostate cancer, Int. Immunopharmacol. 86 (2020), 106709, https://doi.org/10.1016/j.intimp.2020.106709.
[64] D.J. McGrail, et al., High tumor mutation burden fails to predict immune checkpoint blockade response across all cancer types, Ann. Oncol. 32 (5) (2021) 661–672, https://doi.org/10.1016/j.annonc.2021.02.006.
[65] B.T. Fife, J.A. Bluestone, Control of peripheral T-cell tolerance and autoimmunity via the CTLA-4 and PD-1 pathways, Immunol. Rev. 224 (2008) 166–182, https://doi.org/10.1111/j.1600-065X.2008.00662.x.